

Photodeposition of silver on p-Cu₂O/n-TiO₂ nanocomposite applied to visible light degradation of 2,4-dichlorophenol in synthetic wastewater

Alireza Gharaee^a, Azadeh Ebrahimian Pirbazari^{a,b,*}, Ziba Khodaei^c

^aCaspian Faculty of Engineering, College of Engineering, University of Tehran, P.O. Box 43841-119, Rezvanshahr 43861-56387, Iran, email: a.gharaie@ut.ac.ir (A. Gharaee)

^bFouman Faculty of Engineering, College of Engineering, University of Tehran, P.O. Box 43515-1155, Fouman 43516-66456, Iran, Tel. +981334734927; Fax: +981334737228; email: aebrahimian@ut.ac.ir

^cUniversity of Applied Science and Technology, P.O. Box 41635-3697, Guilan, Iran, email: zibakhodaei@uast.ac.ir

Received 25 December 2017; Accepted 7 April 2018

ABSTRACT

This study presents a multicomponent photocatalytic system using simple impregnation-calcination of Cu₂O particles followed by photodeposition of different amounts of Ag on TiO₂ nanoparticles (TCA(a) samples) with high photocatalytic efficiency for 2,4-dichlorophenol (2,4-DCP) degradation under visible light. The obtained samples were characterized through X-ray diffraction, field-emission scanning electron microscopy with energy dispersive X-ray spectroscopy, UV-Vis diffuse reflectance spectroscopy, N₂ physisorption, and transmission electron microscopy techniques. The synthesized samples exhibited a high visible-light photocatalytic activity for 2,4-DCP degradation (50%) compared with pure TiO₂ (28%), which is attributed to the synergetic effect of AgCl, Ag, and Cu₂O on TiO₂ nanoparticles. Furthermore, a dual Z-scheme charge transfer pathway is proposed and discussed for photocatalytic reactions taking place over the prepared photocatalysts. The degradation reactions follow first-order kinetics. Finally, reusing the best photocatalyst (TCA(1.2)) did not result in any decline in its catalyst activity for 2,4-DCP degradation under visible light after four cycles.

Keywords: Z-scheme; Surface plasmon resonance; Cu₂O; Photocatalyst; 2,4-DCP

1. Introduction

Due to the environmental problems related to the treatment of dangerous wastes and polluted waters, rigorous attempts have been recently made to develop a visible light sensitive semiconductor-based photocatalyst that can demonstrate both efficiency and stability features [1–6]. Up to now, titanium dioxide (TiO₂), as one of the important n-type semiconductors, has been the most extensively studied photocatalyst due to its unique properties, such as low cost, chemical stability, and environment-friendly characteristics [7–10]. The major drawback of TiO₂ is its noticeable band gap energy, which is 3.2 eV for anatase [11]. Besides, to excite it in photocatalytic degradation

reactions, it is required to apply UV radiation. In pure TiO₂, once electron–hole pairs are photogenerated, they are recombined easily; leading to a low photocatalytic performance of TiO₂ [12–14]. Several approaches can be employed to improve the photocatalytic performance of TiO₂ under visible light radiation. Among them, coupling TiO₂ with CdS, CdSe, PbS, and WO₃ as narrow band gap semiconductors and producing heterojunctions is an efficient strategy to promote TiO₂ visible-light photocatalytic activity. Through this process, these semiconductors act as visible-light sensitizers to transfer the excited electrons to TiO₂ [15–20]. Cu₂O is a p-type semiconductor with a narrow band gap energy (2.2 eV) [13] and an important visible-light-responsive photocatalyst due to its high visible-light absorption capability, ecofriendly characteristics, low cost, and easy preparation [21–24]. Also, Cu₂O is able to join with

* Corresponding author.

the n-type TiO_2 to generate a p–n heterojunction [25,26], which can extend TiO_2 absorption spectrum to the visible light region and restrain recombination of photogenerated hole–electron pairs. $\text{Cu}_2\text{O}/\text{TiO}_2$ heterojunctions have shown a higher photocatalytic activity compared with pure TiO_2 as the outcome of efficient charge separation between Cu_2O and TiO_2 [27–29]. In semiconductor heterojunction (SH) systems, the electrons and holes have weaker redox abilities and the lower redox ability of electrons and holes due to the shortcoming of the SH has negatively affected photocatalytic reactions [30]. Accordingly, development of photocatalytic systems, which involve fast electron–hole separation and considerable redox ability, is still a challenge. In recent years, Z-scheme photocatalyst system has been employed as an effective strategy for increasing the photocatalytic efficiency due to its unique characteristics [31–36]. In Z-scheme photocatalyst systems, the produced oxidative holes and reductive electrons are restricted to their corresponding valence band (VB) and conduction band (CB), respectively. It results in improvement of charge separation and enhanced redox potential of the photoproducing electrons and holes. However, the competition between typical and Z-scheme charge transfer processes in the SH system is a major problem [37,38]. To solve the competition problem, an electron mediator can be used; however, to prompt the desirable specific carrier transfer the contact resistance of the mediator should be low [29,34,35,38–42]. In Z-scheme photocatalyst systems, Au and Ag metals are doped to work as nanojunctions between the two semiconductors [43,44]. Silver (Ag) has been used as an electron mediator in Z-scheme photocatalyst system because of its low contact resistance or excellent electron conductivity. Due to Ag surface plasmon resonance (SPR) property, its absorption spectra would cover visible light region and the inductively local electric field can accelerate the electron transfer between two semiconductors [45].

In this study, dual Z-scheme p- $\text{Cu}_2\text{O}/\text{Ag}/\text{n-TiO}_2$ photocatalytic system containing different quantities of silver was prepared. In the first step, p- Cu_2O was loaded on TiO_2 nanoparticles by convenient impregnation-calcination of TiO_2 nanoparticles, and silver was deposited on the photocatalyst by adopting a photodeposition method. Structural and morphological properties of p- $\text{Cu}_2\text{O}/\text{Ag}/\text{n-TiO}_2$ samples were investigated by X-ray diffraction (XRD), field-emission scanning electron microscopy with energy dispersive X-ray spectroscopy (FESEM/EDX), UV-Vis diffuse reflectance spectra (DRS), N_2 physisorption, and transmission electron microscopy (TEM) techniques. By employing the photocatalytic degradation of 2,4-dichlorophenol (2,4-DCP), as a model reaction, photoactivity performance of the synthesized nanocomposites was evaluated. Chlorophenols are toxic chemicals that are used in many industrial applications such as petrochemicals, pesticide, dye intermediates, and paint [46]. Especially, 2,4-DCP is an important chemical precursor for the manufacture of a widely used herbicide, 2,4-dichlorophenoxy acetic acid [47]. However, 2,4-DCP may cause some pathological symptoms and changes to human endocrine systems, after entering from the skin and gastrointestinal tract. Recently, concerns have been raised because of chlorophenols persistence and bioaccumulation both in animals and in humans [48–50]. Consequently, innovative and

effective ways should be developed to minimize the harm of chlorophenols in the environment. To the best of our knowledge, this is the first report on the preparation of p- $\text{Cu}_2\text{O}/\text{n-TiO}_2$ systems possessing different amounts of silver. The outstanding properties associated with these samples suggested that they can be employed as a novel visible-light harvesting catalyst for given applications in photocatalysis. The p- $\text{Cu}_2\text{O}/\text{Ag}/\text{n-TiO}_2$ samples exhibited an improved efficiency for 2,4-DCP photocatalytic degradation under visible light.

2. Experimental

2.1. Materials

Tetraisoopropylorthotitanat (TIP, Merck no. 8.21895), anhydrous ethanol, and high-purity 2,4-DCP (98%, Merck no. 803774) consumed for photocatalytic experiments as probe molecules were purchased from Merck company, Germany. Silver nitrate (AgNO_3 , 99.9%) was obtained from Merck (no. 101510). Copper(II) nitrate trihydrate ($\text{Cu}(\text{NO}_3)_2 \cdot 3\text{H}_2\text{O}$) was purchased from Merck (no. 102753). Acetic acid (Merck no. 1.00063) and methanol (Merck no. 106007) were applied to prepare the samples. All used reagents were of analytic grade and applied without additional purification. For the preparation of all aqueous solutions, double distilled water was used.

2.2. TiO_2 nanoparticles synthesis

To prepare TiO_2 nanoparticles, first, 4 mL of TIP was mixed with 70 mL anhydrous ethanol followed by ultrasonication (ELMA-Germany, E60H, ultrasound bath) for 1 h to form solution A. Meanwhile, 3 mL of acetic acid was diluted to 90 mL deionized water to form solution B. Next, solution B was dropped into solution A at the speed of one drop per 3 s at 50°C with stirring. Subsequently, the mixture solution was stirred for 30 min, continuously. Finally, after cooling the solution to room temperature, the solid product was separated from the suspension, washed with deionized water and ethanol for several times, and then dried up in vacuum for 12 h at 60°C. The resulting powder was annealed at 300°C under N_2 atmosphere for 1 h to TiO_2 nanoparticles.

2.3. Preparation $\text{TiO}_2/\text{Cu}_2\text{O}$ nanocomposite

To prepare $\text{TiO}_2/\text{Cu}_2\text{O}$ nanocomposite [45], 0.3 g of TiO_2 nanoparticles were immersed in a $\text{Cu}(\text{NO}_3)_2$ solution consisting of 4.5 mg $\text{Cu}(\text{NO}_3)_2 \cdot 3\text{H}_2\text{O}$ and 20 mL deionized water. The mixed solution was stirred at 80°C until the solvent was thoroughly evaporated. The resultant powder was calcined at 350°C for 4 h to yield $\text{Cu}_2\text{O}/\text{TiO}_2$ nanocomposite; and the sample was labeled as TC.

2.4. Photodeposition Ag nanoparticles on $\text{TiO}_2/\text{Cu}_2\text{O}$ nanocomposite

In this step [45], 0.3 g of $\text{Cu}_2\text{O}/\text{TiO}_2$ powder and different amounts of AgNO_3 (1.2, 2.4, and 4.8 mg) were added to 16 mL deionized water under magnetic stirring. Then, 4 mL of methanol was injected into the supernatant. The obtained solution was irradiated by a UV-Vis lamp for 2 h. After that,

the precipitate was filtered and completely rinsed three times with deionized water and ethanol to remove the residual impurities. Then, these samples will be shown as TCA(a), where (a) represents the amount of AgNO_3 used during the synthesis of TCA samples.

2.5. Photodeposition Ag nanoparticles on TiO_2

In this step, 0.3 g of TiO_2 powder and 2.4 mg of AgNO_3 were added into 16 mL deionized water under magnetic stirring. Then, 4 mL methanol was injected into the above suspension, followed by the irradiation of a UV-Vis light lamp for 2 h. Next, the suspension was collected and thoroughly rinsed with deionized water and ethanol three times to remove the residual impurity. Then, this sample will be shown as TA.

2.6. Characterization

The XRD patterns were recorded by a Siemens D5000 instrument (Germany), while Cu K_α radiation was employed as the X-ray source. The diffractograms were recorded within the 2θ range of 20° – 80° . Morphology of the samples was identified by a scanning electron microscopy (Vegall-Tescan Company, Czech Republic) equipped with an energy dispersive X-ray (EDX) detector. The DRS of the samples were recorded by an Ava Spec-2048TEC spectrometer. The microstructure and morphology of the prepared samples were investigated by a TEM (Philips CM30 300 kV). Physisorption of nitrogen was studied by a Quantachrome Autosorb-1-MP (Micromeritics) in order to measure Brunauer–Emmett–Teller (BET) areas through static nitrogen physisorption from -196°C to 200°C until the pressure reached below 5 mbar.

2.7. Photocatalytic degradation of 2,4-DCP

2,4-DCP was selected as a model of organic pollutants to examine the efficiency of the obtained samples in photocatalytic processes. Two irradiation sources with illumination power in the UV and visible region was used. For UV region experiments, 400 W Kr lamp was used (Osram, Germany), with 90% illumination power in the UV-A region (400–315 nm) and about 10% in the UV-B region (315–280 nm). For visible light experiments, halogen was used, ECO OSRAM 500 W lamp (350–800 nm, with the most intense peak at 575 nm). In each photocatalytic degradation experiment, the beaker containing optimum amount of photocatalyst and 100 mL of 2,4-DCP aqueous solution (40 mg/L) was stirred first for 10 min under dark for desorption/adsorption equilibrium, followed by keeping it under light irradiation for 180 min. At certain times, 2 mL of the solution was taken and filtered to eliminate the photocatalyst and analyzed using Rayleigh UV-2601 UV/VIS spectrophotometer ($\lambda_{\text{max}} = 227$ nm). The calibration curve at $\lambda_{\text{max}} = 227$ nm in the concentration range (1–50 mg/L) of 2,4-DCP and calculated % removal of 2,4-DCP using equation:

$$\% \text{ Removal} = ((C_i - C_t) / C_i) \times 100 \quad (1)$$

where C_i and C_t (mg/L) are the initial concentration and the concentration of 2,4-DCP at time t , respectively.

2.8. Statistical analysis

All experiments were performed in duplicate and the mean values were presented. The data were analyzed by one-way analysis of variance using SPSS11.5 for Windows. The data were considered statistically different from control at $P < 0.05$.

3. Results and discussion

3.1. Crystallographic properties

XRD results of the synthesized samples are presented in Fig. 1, where all the diffraction peaks of the as-prepared samples match well with the standard PDF cards. The strong diffractions at $2\theta = 25.3^\circ, 37.7^\circ, 48.0^\circ, 53.8^\circ, 55.0^\circ$, and 62.6° can be assigned to the diffractions from anatase TiO_2 (JCPD file: 21-1272). For pure Cu_2O , the diffraction peaks at $2\theta = 29.2^\circ, 36.5^\circ, 43.1^\circ, 61.8^\circ, 74.2^\circ$, and 77.6° were indexed to (110), (111), (200), (220), (311), and (222) planes of cubic Cu_2O (JPDFS 34-1354) [51]. In the XRD pattern of TC sample (Fig. 1(b)), the weak reflection peak observed at approximately 36.5° was indexed to (111) Cu_2O crystal planes (JCPDS file: 65-3288). Aside from the diffraction peaks of TiO_2 nanoparticles, no other peaks were observed on the surface of this sample (Fig. 1(b)). Also, no Cu (35.49° and 38.73° characteristic peaks) or CuO (43.29° and 50.43° characteristic peaks) phase is observed. Since Cu_2O was fabricated on TiO_2 nanoparticles, it has no influence on the TiO_2 lattice. No other diffraction peaks of Cu_2O can be observed, probably because of the low loading amount, the small size of its particles, and its good dispersion. Fig. 1(c) shows the XRD pattern of TA sample. The diffractions at 2θ of 32.2° and 46.2° are indexed to AgCl nanoparticles. The diffractions at about $2\theta = 32.2^\circ, 46.21^\circ, 57.51^\circ$, and 67.4° can be related to AgCl phase (JCPDS no. 85-1355). Formation of AgCl can be attributed by using methanol as a solvent during the photodeposition of silver, the presence of Cl^- impurity, and application of AgNO_3 . Four diffractions were reported at $2\theta = 38.048^\circ, 44.133^\circ, 64.303^\circ$, and 77.326° for silver in the standard powder diffraction card of JCPDS, file no. 04-0783. Due to the low amount, small crystallite size, or high distribution of Ag particles, the main diffractions of metallic Ag in XRD pattern of the TA sample was not detected. Figs. 1(d)–(f) illustrate the XRD patterns of TCA(a) samples. The major diffraction of TiO_2 and some diffractions for AgCl ($2\theta = 32.2^\circ$ and 46.2°), metallic Ag nanoparticles ($2\theta = 44.2^\circ$), and Cu_2O ($2\theta = 36.5^\circ$) was detected. These diffractions can prove the presence of metallic Ag and AgCl nanoparticles and also Cu_2O and TiO_2 in the TCA(a) samples.

The mean TiO_2 crystal size at $2\theta = 25.3^\circ$ using Scherrer's equation for each of samples was calculated [52]:

$$D = K\lambda / \beta \cos\theta \quad (2)$$

In this equation, D denotes sample mean crystal size, λ is the wavelength (1.54056 Å) of the X-ray source, β is diffraction full width at half maximum in radian, θ is the diffraction angle regarding the peak maximum, and K is a constant (0.89). The TiO_2 crystal size in all the obtained nanocomposites is in the range of nanosized (Table 1).

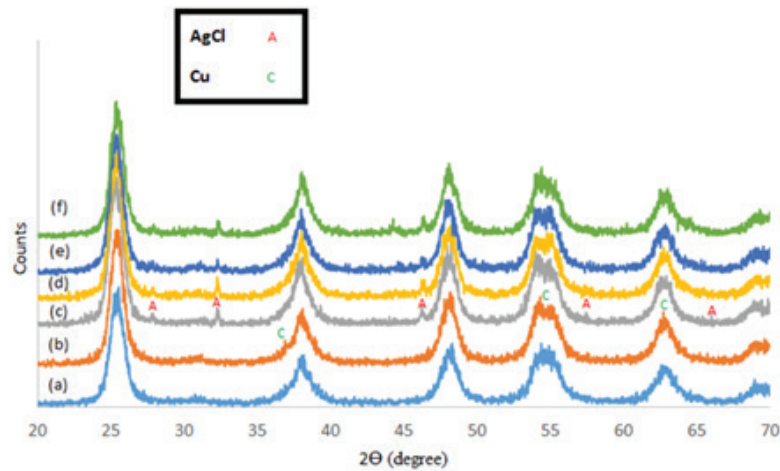


Fig. 1. XRD patterns of (a) T, (b) TC, (c) TA, (d) TCA(1.2), (e) TCA(2.4), and (f) TCA(4.8).

Table 1
Phase, crystal size, and lattice parameters of the prepared samples

Sample	Phase	Crystal size (nm)	$a = b$ (Å)	c (Å)	Cell volume (Å ³)
T	Anatase	7.117	3.770	9.129	129.749
TC	Anatase	7.908	3.778	9.129	130.301
TA	Anatase	7.484	3.774	10.000	142.431
TCA(1.2)	Anatase	7.908	3.774	9.535	135.808
TCA(2.4)	Anatase	7.900	3.784	9.806	140.409
TCA(4.8)	Anatase	7.900	3.784	9.535	136.528

The lattice parameters ($a = b \neq c$) corresponding to tetragonal crystalline structure were obtained for (101) crystal plane of anatase phase using Eq. (3):

$$1/d^2 = (h^2 + k^2)/a^2 + l^2/c^2 \quad (3)$$

Considering the interplanar spacing (d_{hkl}), the distance between adjacent planes in the set (hkl) can be determined using the Bragg law:

$$d_{hkl} = \lambda/2\sin\theta \quad (4)$$

The cell volume (tetragonal one) was calculated as:

$$V = a^2c \quad (5)$$

where a and c are considered as lattice parameters. Table 1 shows the lattice parameters of the samples.

The obtained values of TiO₂ lattice parameters in the prepared samples are in good agreement with TiO₂ anatase structure (Joint Committee for Powder Diffraction Standard, 78-2486). An increase in TiO₂ crystal size and cell volume for TA and TCA(a) samples due to the diffusion of Ag ion into TiO₂ lattice during the photodeposition process was observed. A significant difference between ionic radii of the dopant and the host ions (i.e., Ag⁺: 1.260 Å and Ti⁴⁺: 0.605 Å) is expected to cause enhancement of the

TiO₂ cell volume. Jun et al. [53] worked on silver-doping induced lattice distortion in TiO₂ nanoparticles and reported that the values of a , c , and V for the rutile and anatase phases significantly increase with Ag-doping. Compared with the rutile phase, there is a larger expansion for the anatase lattice with Ag-doping, suggesting that Ag-doping imposes an effect dominantly on the anatase phase in TiO₂.

3.2. Diffuse reflectance spectroscopy

The obtained diffuse reflectance (DR) spectra of the samples over 200–800 nm are shown in Fig. 2(A). There is a broad intense absorption peak at about 400 nm in the DR spectra of all the samples because of charge-transfer originating from VBs of the samples. This transfer is caused by the 2p orbitals of the oxide anions to the CB formed by 3d t_{2g} orbitals of the Ti⁴⁺ cations [54]. In particular, the samples TA, TC, and TCA(a) exhibit an enhanced light absorption compared with the pure TiO₂ within the range of 400–800 nm. This observation indicates that loading Cu₂O and Ag can improve visible-light absorption by the samples that promote TiO₂ photocatalytic activity. In the DR spectra of TA and TCA(a) samples, the absorption shoulder peak can be observed within the range between 360 and 500 nm. These absorption shoulders result from the postbroadening SPR peak [55]. Visible region of

the spectra is associated with the localized SPR that would enable these samples to show broad and strong absorption [56,57]. In addition, TCA(2.4) and TCA(4.8) samples exhibit a stronger light absorption compared with TCA(1.2) sample, due to the fact that they contain a higher Ag percentage and have darker color compared with TCA(1.2) (Table 3, EDX results). The band gap energy of the samples from the DR spectra was calculated for the synthesized samples according to Eq. (6) [58]:

$$[F(R) hv]^{0.5} = A (hv - E_g) \quad (6)$$

where A is a constant, $F(R)$ is the Kubelka–Munk function, and E_g is the band gap. The E_g data of the samples are presented in Table 2. The TCA(a) samples band gap decreased compared with that of TiO_2 (Table 3). It is apparent that Ag

loading on the TiO_2 surface affects the TiO_2 optical properties significantly. Moreover, it is seen that the photoresponse of the TCA(a) nanocomposite is greatly shifted to visible light ranges because of the SPR properties of silver nanoparticles, while pure TiO_2 band gap (2.90 eV) is narrowed to 2.61 eV. Also, the coupling of Cu_2O is very effective on the band gap of TiO_2 . It can be noticed that the absorption band edge of Cu_2O ($E_g = 2.20$ eV [13]) component in $\text{Cu}_2\text{O}/\text{TiO}_2$ nanocomposite ($E_g = 2.75$ eV) is blue-shifted to the short wavelength compared with that of pure Cu_2O . The estimated band gap of $\text{Cu}_2\text{O}/\text{TiO}_2$ nanocomposite is 2.75 eV, which is lower than band gap of pure TiO_2 (2.90 eV) and higher than pure Cu_2O band gap (2.20 eV). These results demonstrate that the interfaces are closely combined and the band edges are matched well between TiO_2 and Cu_2O semiconductors. Therefore, harvesting visible light and efficiency of charge carrier

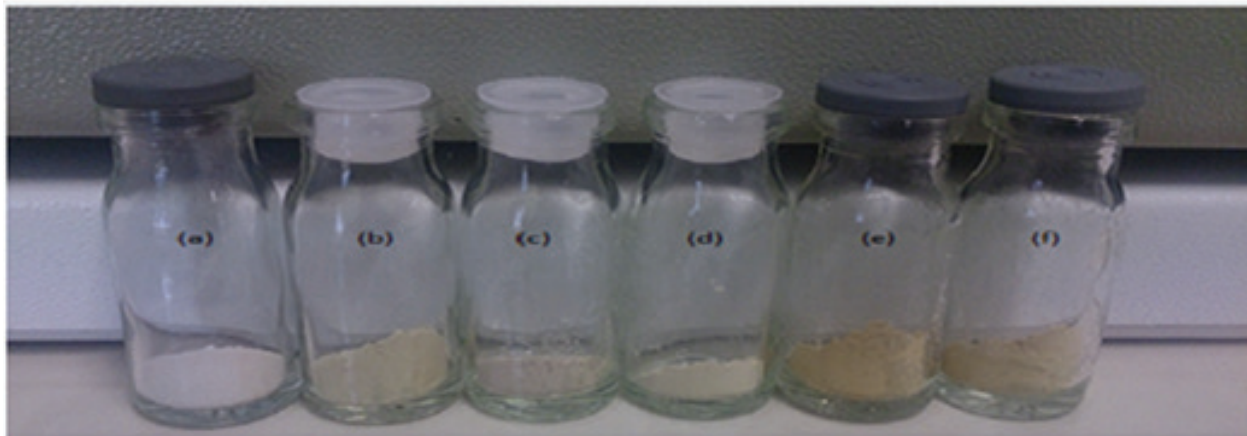
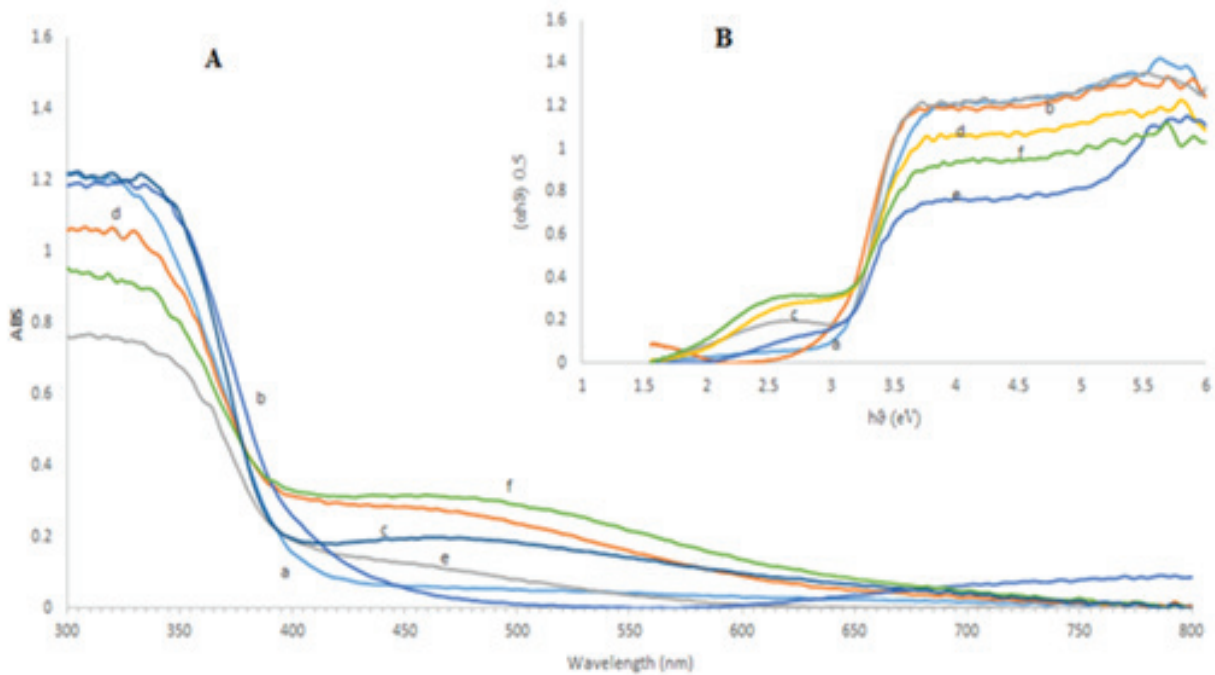


Fig. 2. (A) Diffuse reflectance spectra and (B) Kubelka–Munk plots for the band gap energy calculation of (a) T, (b) TC, (c) TA, (d) TCA(1.2), (e) TCA(2.4), and (f) TCA(4.8).

separation might be achieved more easily for $\text{Cu}_2\text{O}/\text{TiO}_2$ and TCA(a) samples. The Kubelka–Munk curves for the synthesized samples are exhibited in Fig. 2(B).

3.3. FESEM/EDX and TEM analyses

FESEM images with different magnifications in Figs. 3 and 4 reveal the microstructure and morphology of the prepared samples. In the FESEM image of TC sample, two morphologies related to Cu_2O and TiO_2 presence in this sample were detected. Accordingly, the particle size of pure TiO_2 is around 9–20 nm. In the FESEM results of TA and TCA(a) samples, nanoparticles with the size in the range of around 155–375 nm was observed. These AgCl nanoparticles are formed during Ag photodeposition on TiO_2 surface and TC samples. The EDX results were applied to evaluate the prepared samples elemental composition (Fig. 5 and Table 3). The obtained EDX analysis data verify the existence of C, Ti, O, Cu, and Ag in the prepared samples. In the EDX spectra of TA and TCA(a) samples, the absorption peak at 3 keV corresponds to metallic silver in the prepared samples [59]. Elemental mapping (Fig. 6) shows that C, Ti, O, Cu, and Ag elements are dispersed uniformly in the testing area, suggesting the uniform distribution of Cu_2O and Ag nanoparticles over the surface of TiO_2 . Fig. 7 shows the TEM image with different magnifications of the best photocatalyst in this work (TCA(1.20) nanocomposite). These images showed heterojunction of Cu_2O and TiO_2 , in addition to Ag and AgCl nanoparticles, in this sample.

3.4. N_2 physisorption analysis

N_2 adsorption–desorption isotherm results are shown in Fig. 8. The acquired sorption isotherms relating to the all prepared samples suggest the type IV isotherm according to

Table 2
Band gap energy of the prepared samples

Sample	E_g (eV)
T	2.90
TC	2.75
TA	2.90
TCA(1.2)	2.65
TCA(2.4)	2.79
TCA(4.8)	2.61

Table 3
Elemental chemical analysis of the prepared samples

Sample	C (wt%)	N (wt%)	O (wt%)	Ti (wt%)	Cu (wt%)	Ag (wt%)
T	3.76	9.01	43.4	43.83	–	–
TC	4.79	7.14	31.71	56.04	0.33	–
TA	11.48	14.04	32.48	34.47	–	7.53
TCA(1.2)	6.08	13.03	43.55	32.10	0.42	4.83
TCA(2.4)	6.19	11.31	32.21	42.00	0.53	7.76
TCA(4.8)	5.56	10.03	38.70	38.06	0.30	6.75

IUPAC classification [60]. Textural and structural parameters of the obtained samples are shown in Table 4. Specific surface areas and average pore diameter were calculated based on BET analysis, while pore volumes were determined from the desorption branch of Barrett–Joyner–Halenda model. BET surface area of TCA(a) samples is far greater than the starting material (TC sample), indicating the loading of Ag and AgCl nanoparticles on TC surface.

3.5. Photocatalytic activity evaluation

The photoactivity performance of the synthesized samples was investigated for 2,4-DCP degradation, as a model of organic pollutant, under visible and UV irradiation (Figs. 9 and 10). Upon UV/visible irradiation, TCA(1.2) photocatalyst showed the highest performance among the TCA(a) samples and achieved about 60% and 50% degradations, respectively, after 180 min irradiation. Under UV irradiation, pure TiO_2 and other photocatalysts showed the higher photoactivity compared with their activity under the visible light as a result of higher photoenergy of UV irradiation than visible light. It can be clearly seen that the loading components (Ag and Cu_2O in this work) have significant impact on TiO_2 photocatalytic activity under visible light. As compared with TiO_2 , both samples TA and TC exhibit remarkably improved photocatalytic activity, demonstrating that Ag and Cu_2O can be used as cocatalysts to achieve promoted photocatalytic activity. Importantly, good activity for TCA(a) samples compared with TiO_2 under visible light was observed, as an outcome of Ag and Cu_2O synergetic effect on TiO_2 photocatalytic activity. Also, the TCA(a) samples displayed a higher photocatalytic performance compared with TC sample. Here, we assume that the photo-induced charge transfer in TC obeys the typical charge transfer mechanism of SHs. When Cu_2O and TiO_2 are excited, CB electrons of Cu_2O will transfer to TiO_2 CB, and meanwhile, TiO_2 VB holes will transfer to Cu_2O VB. Consequently, the hole density in TiO_2 VB is declined while it is enhanced in Cu_2O VB. Due to the less positive position of Cu_2O VB, Cu_2O holes do not have enough energy to oxidize OH^- or H_2O to form OH^* . Hence, the rate of OH^* generation by the sample TC is low. Based on this results, a probable photocatalytic mechanism of the TCA(a) samples is proposed in Fig. 11. Under UV-Vis irradiation, both Cu_2O and TiO_2 are photoexcited to give electrons and holes. Since Fermi level equilibration would establish at the interfaces located between TiO_2 , Ag, and Cu_2O particles, before light irradiation, and electrons on TiO_2 CB will migrate to Ag after light irradiation. Furthermore, intense

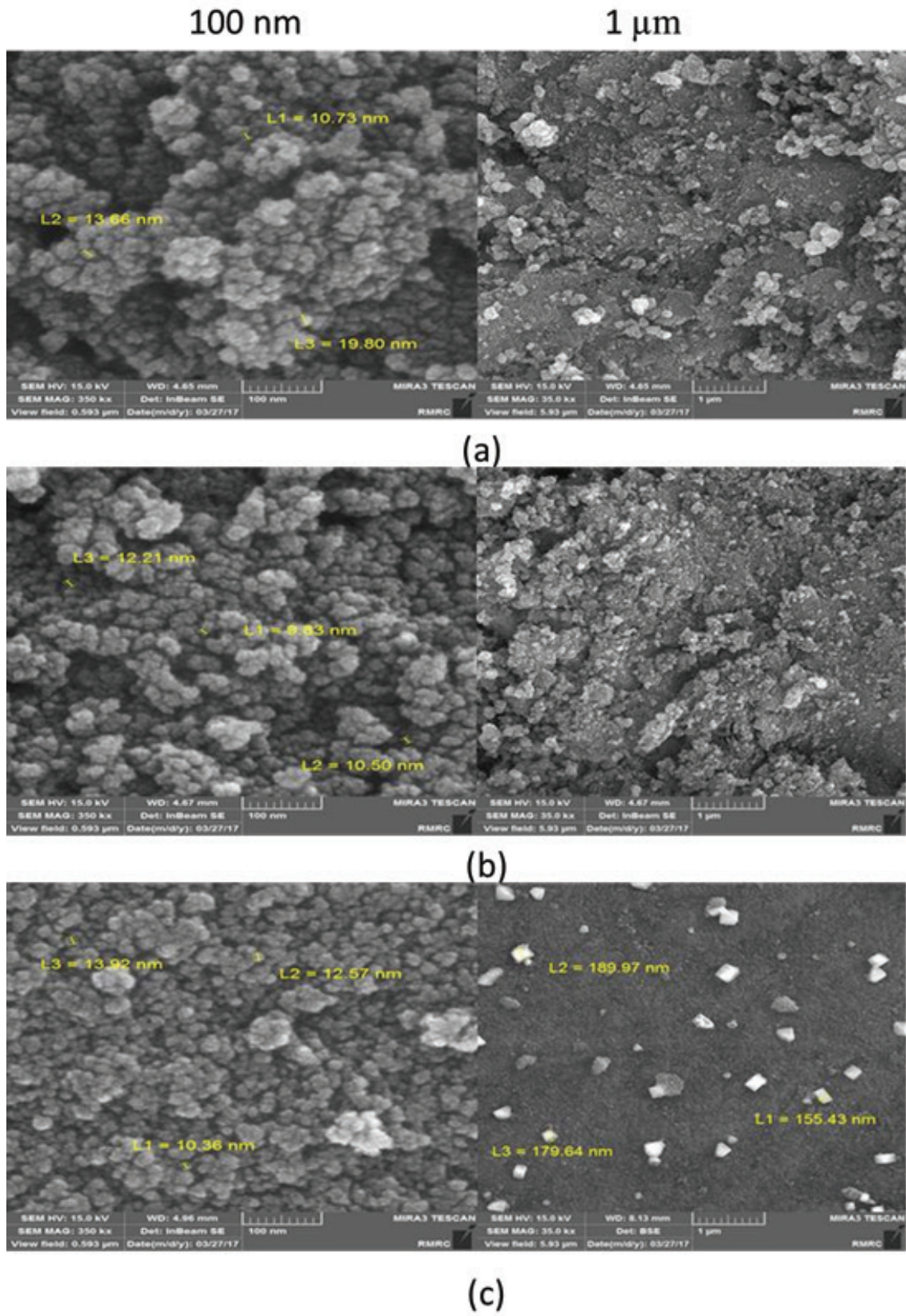


Fig. 3. FESEM images of (a) T, (b) TC, and (c) TA.

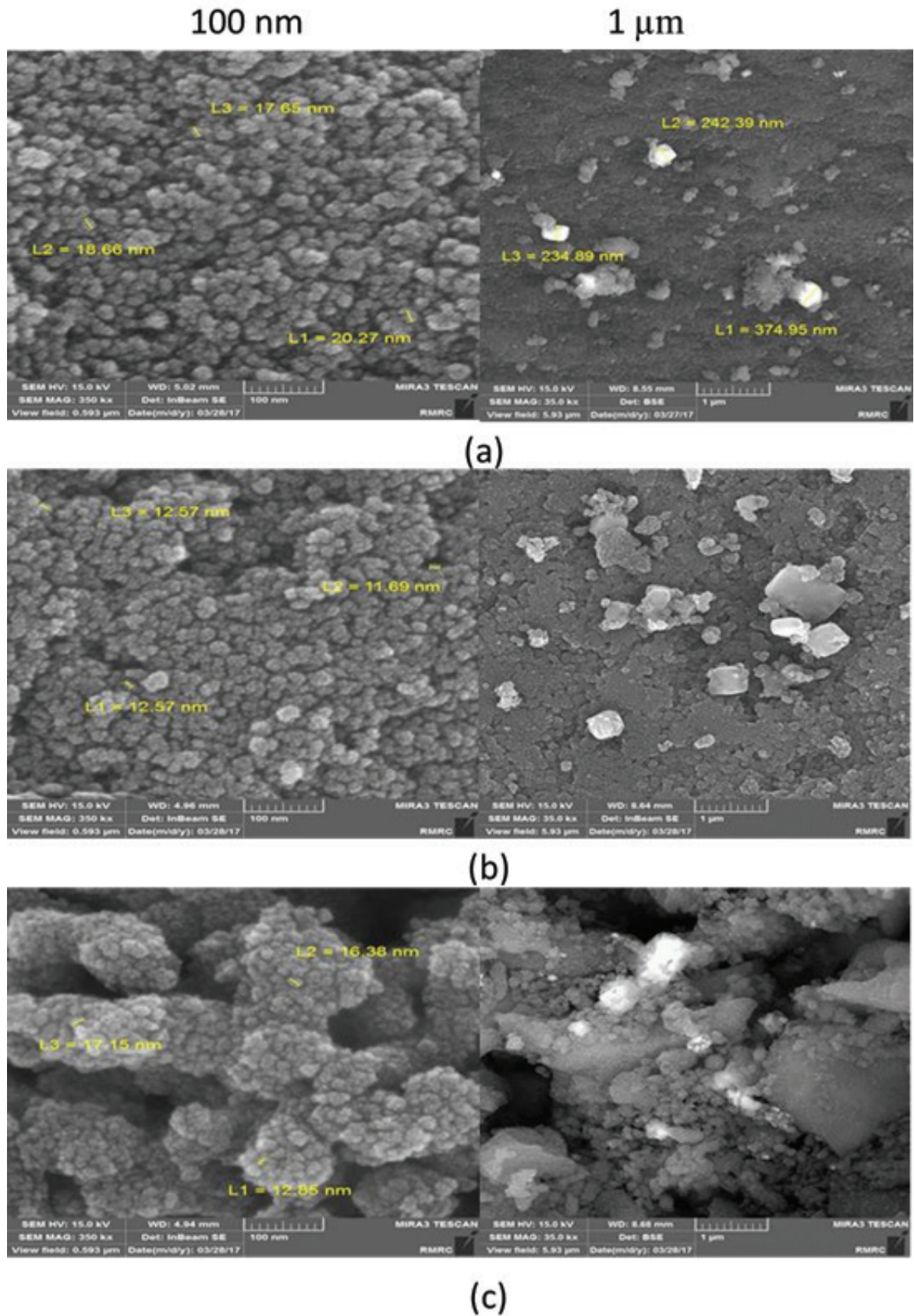


Fig. 4. FESEM images of (a) TCA(1.2), (b) TCA(2.4), and (c) TCA(4.8).

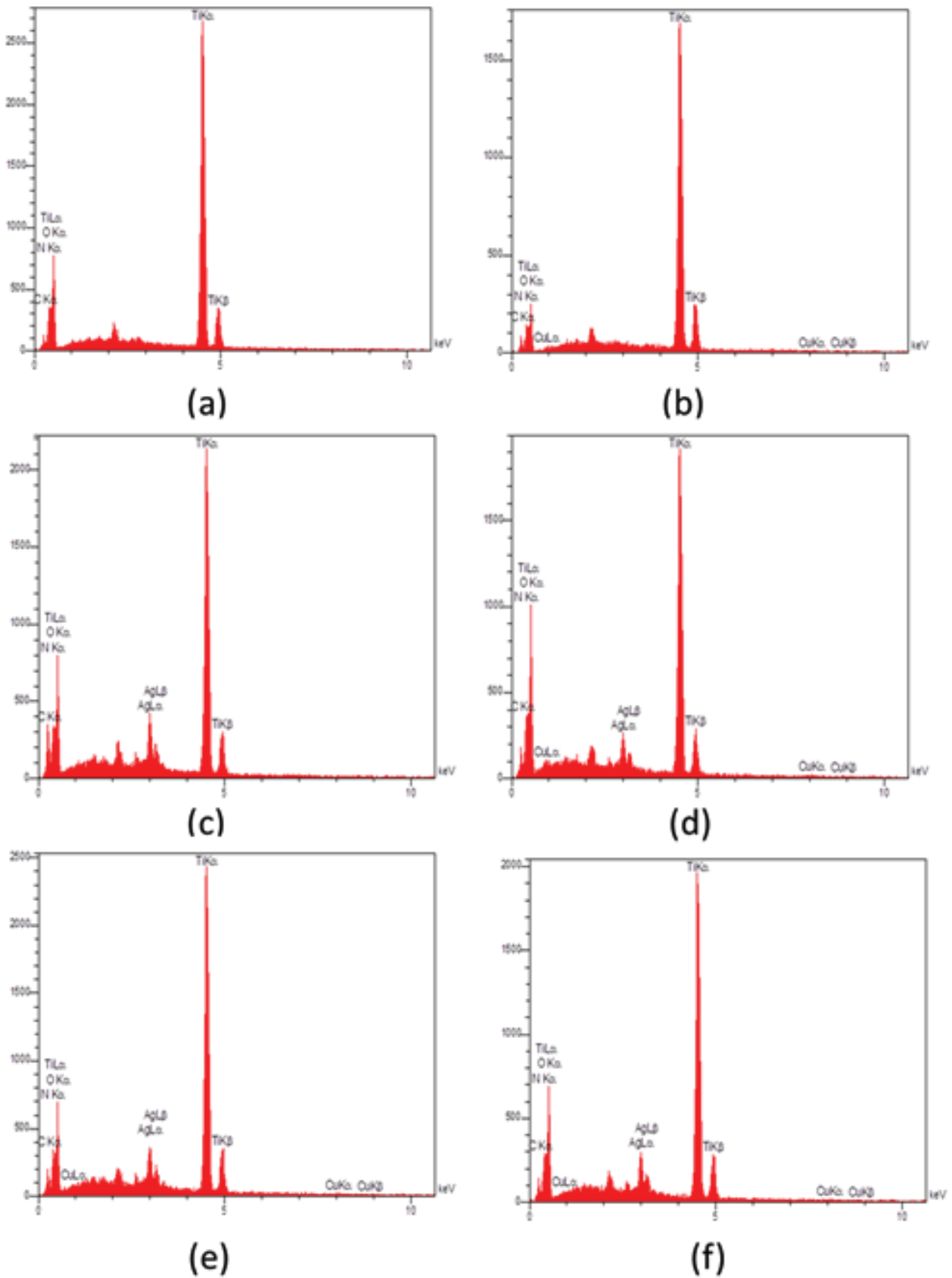


Fig. 5. EDX spectra of (a) T, (b) TC, (c) TA, (d) TCA(1.2), (e) TCA(2.4), and (f) TCA(4.8).

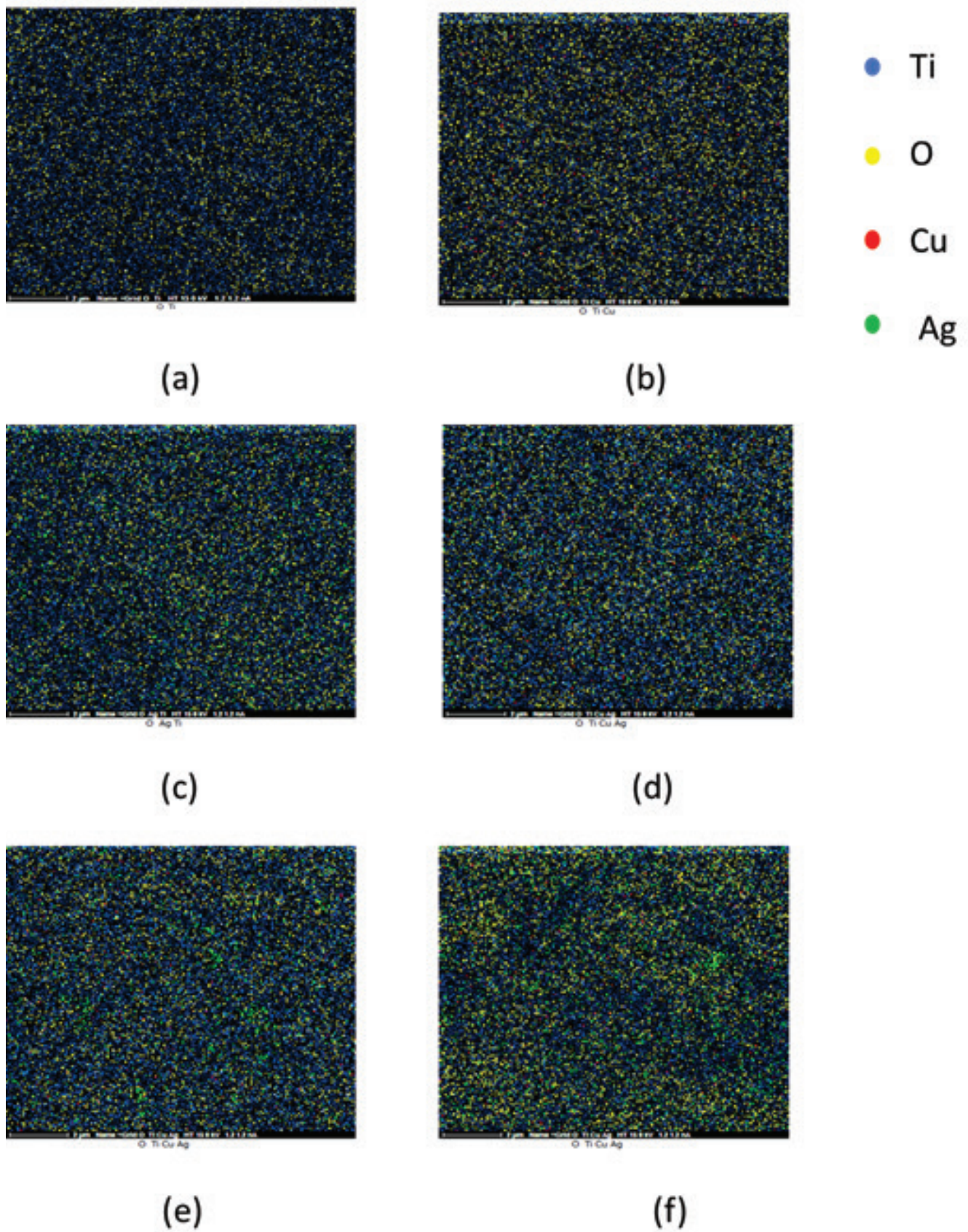


Fig. 6. Elemental mapping of (a) T, (b) TC, (c) TA, (d) TCA(1.2), (e) TCA(2.4), and (f) TCA(4.8).

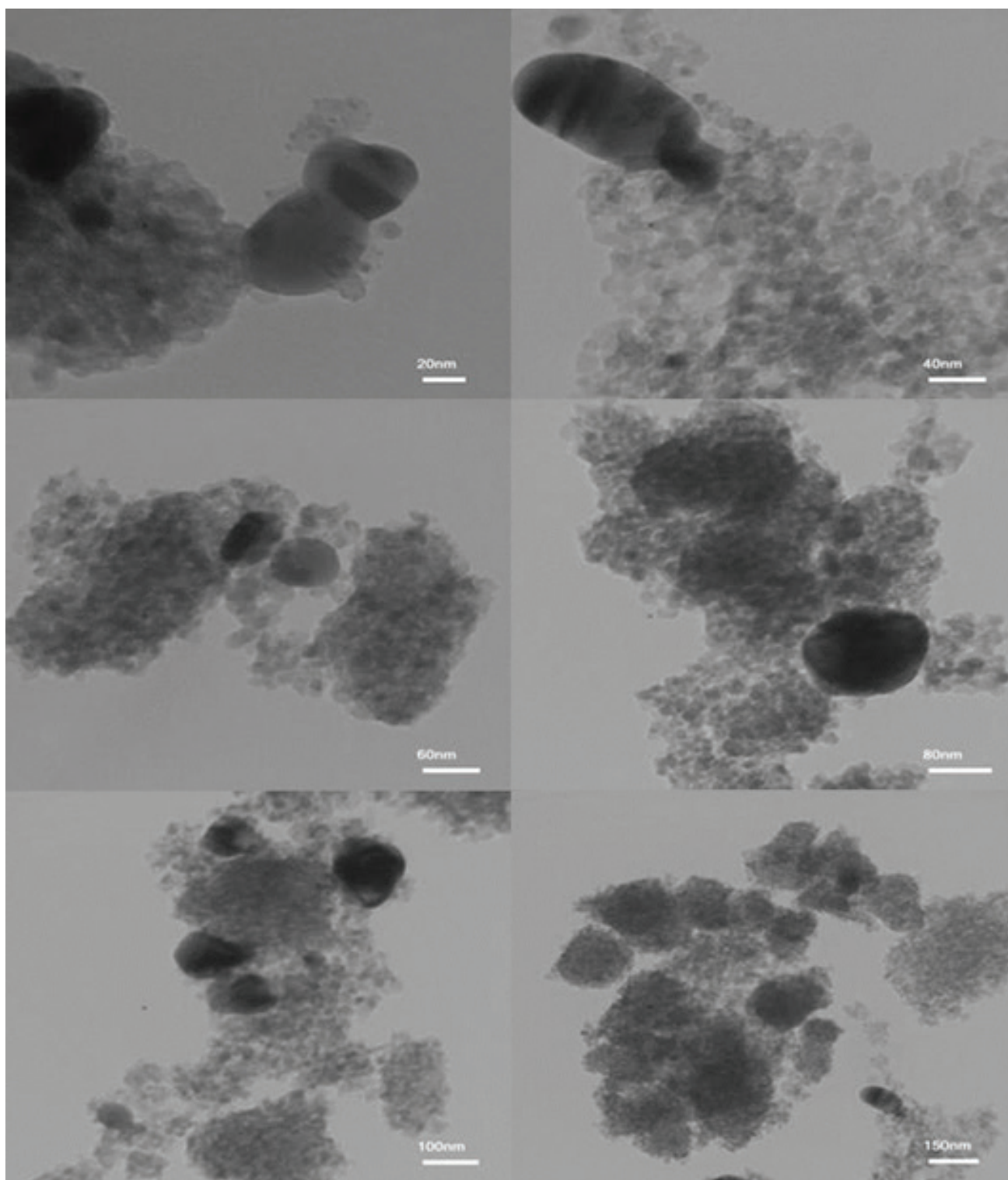
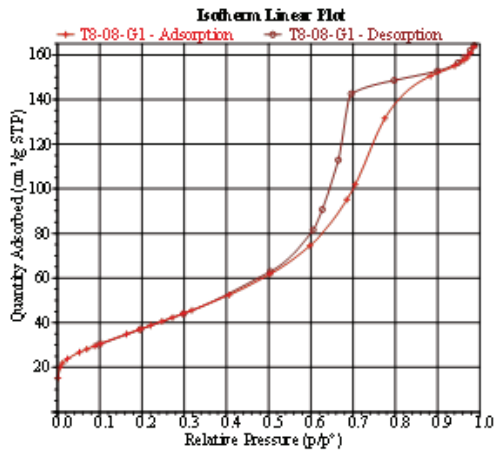


Fig. 7. TEM image of TCA(1.2) nanocomposite with different magnifications.

SPR of Ag nanoparticles would contribute to the enhanced local electric field around the interfaces, which can advance Ag electrons to inject into Cu_2O VB and recombine with holes or into Cu_2O CB via direct electron transfer or plasmon-induced resonant energy transfer [61]. It is noteworthy

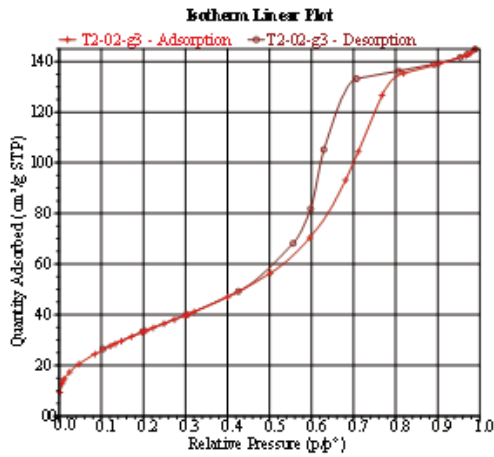
that this kind of charge transfer retains the photogenerated holes on the more positive TiO_2 VB and electrons on the more negative Cu_2O CB, which not only improves separation of electron-hole pairs dramatically but more importantly can preserve their high redox ability [38,62]. Since such charge



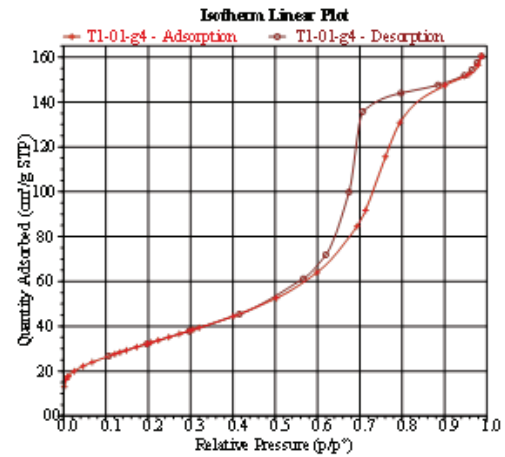
(a)



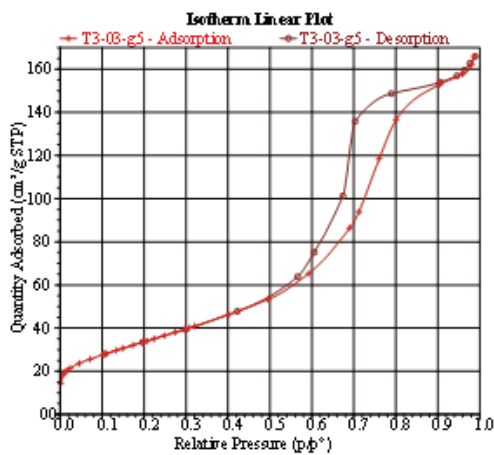
(b)



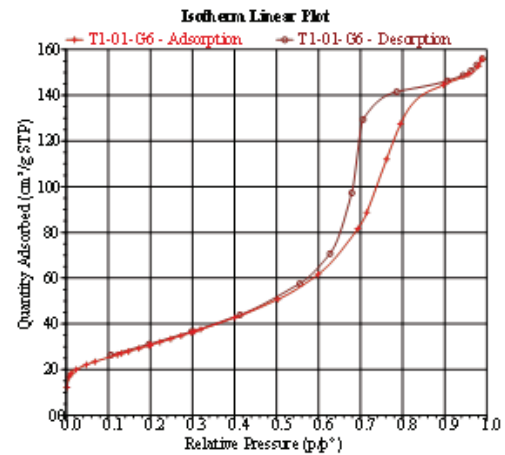
(c)



(d)



(e)



(f)

Fig. 8. N₂ adsorption–desorption isotherms for (a) T, (b) TC, (c) TA, (d) TCA(1.2), (e) TCA(2.4), and (f) TCA(4.8).

transfer mechanism is similar to Z-scheme mechanism in a double “Z” shape, and hereby tentatively call it as “dual Z-scheme charge transfer.” In this photocatalyst system, the left holes in TiO₂ can transfer to the AgCl surface due to the negative surface charge [58], which could cause the oxidation of Cl⁻ ions to Cl⁰ atoms [63–67]. Due to high oxidation potency of the chlorine atoms, the 2,4-DCP could be oxidized by the chlorine atoms and hence the Cl⁰ could be

reduced to chloride ions again. Also, the holes could react with H₂O to form hydroxyl radicals. Both hydroxyl radicals and chlorine atoms were highly reactive species for effective degradation of 2,4-DCP (Fig. 11).

Table 4
Textural and structural parameters of the prepared sample

Sample	S _{BET} (m ² /g)	Average pore diameter (nm)	Pore volume (cm ³ /g)
T	139.862	6.943	0.260
TC	31.047	7.908	0.065
TA	130.482	6.720	0.226
TCA(1.2)	121.711	7.749	0.251
TCA(2.4)	125.994	7.743	0.260
TCA(4.8)	115.096	8.041	0.244

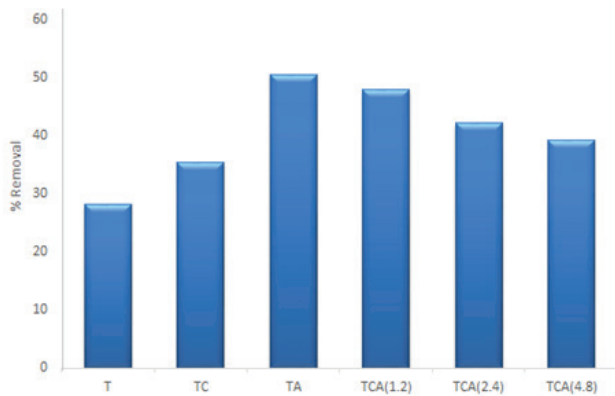


Fig. 9. Photocatalytic degradation of 2,4-DCP in the presence of the prepared samples under visible light. (Initial concentration of 2,4-DCP, 40 mg/L; volume, 100 mL; catalyst dosage, 20 mg.)

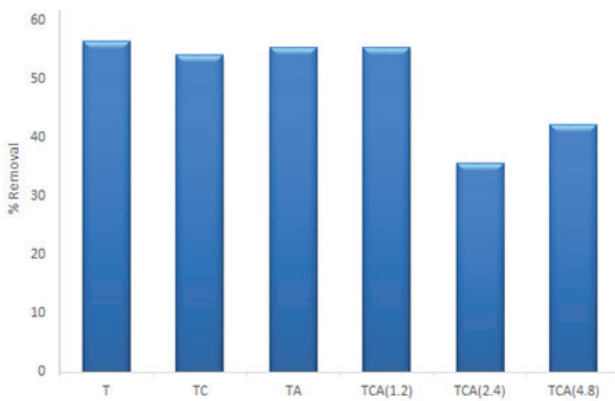


Fig. 10. Photocatalytic degradation of 2,4-DCP in the presence of the prepared samples under UV irradiation. (Initial concentration of 2,4-DCP, 40 mg/L; volume, 100 mL; catalyst dosage, 10 mg.)

3.6. Kinetic study

The kinetic parameters for the elimination of 2,4-DCP are shown in Fig. 12 and Table 5. The obtained results show that the reaction is first-order, which means that its kinetics can be expressed as $\ln(C_0/C) = k_{obs} t$. In this equation, k_{obs} (min⁻¹) is the apparent rate constant, C_0 and C are 2,4-DCP initial concentration and concentration at reaction time t , respectively. The initial rate of reaction by production of k_{obs} in initial concentration of 2,4-DCP was calculated (Table 5). The initial rate of reaction in 2,4-DCP photocatalytic degradation is faster for higher 2,4-DCP initial concentrations. These results may be explained by the short lifetime of active species formed during the reaction. The active oxygen species such as OH[•] and O₂^{•-} are formed on TCA(1.2) surface, which could not diffuse away and would interact with 2,4-DCP molecules at the photocatalyst surface.

3.7. Recyclability of TCA(1.2) photocatalyst

The recyclability of photocatalyst is important characteristics for developing heterogeneous photocatalysis process for wastewater treatment since it could contribute

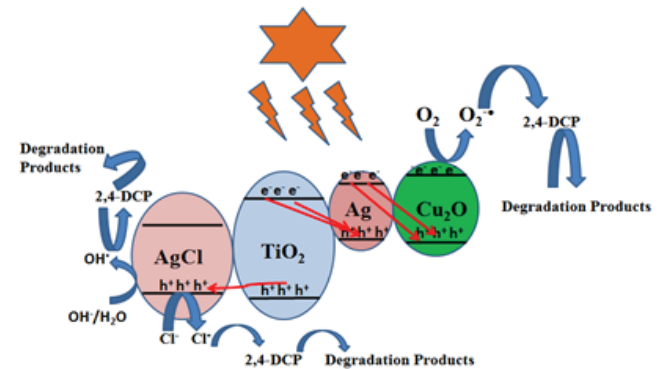


Fig. 11. The proposed mechanism for photocatalytic degradation of 2,4-DCP over TCA(1.2).

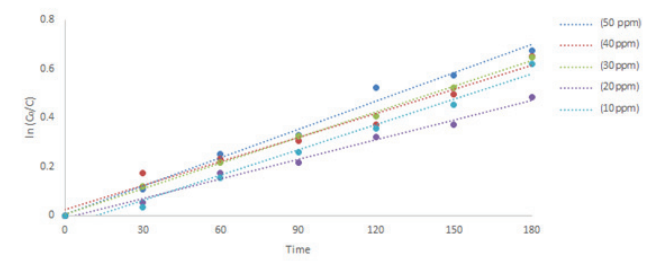


Fig. 12. The effect of initial concentration on the photocatalytic degradation rate of 2,4-DCP over TCA(1.2) photocatalyst.

Table 5
First-order reaction rate constants and correlation coefficients for different concentrations of 2,4-DCP

Concentration (mg/L)	R^2	k_{obs} (min^{-1})	Initial reaction rate ($\text{mg/L} (\text{min}^{-1})$)	$t_{1/2}$ (min)
10	0.9837	0.0035	0.035	198.0
20	0.9901	0.0037	0.074	187.3
30	0.998	0.0035	0.105	198.0
40	0.9735	0.0033	0.132	210.0
50	0.9872	0.0038	0.190	182.40

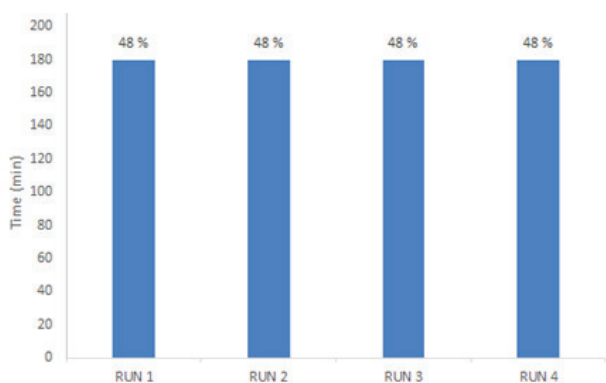


Fig. 13. Recyclability of the TCA(1.2) for photocatalytic degradation of 2,4-DCP after four successive cycles (catalyst dose: 20 mg; 2,4-DCP: 40 mg/L).

significantly to reduce the operational cost. The recyclability of the TCA(1.2) nanocomposite was examined by applying the same 2,4-DCP photocatalytic degradation in four repeated cycles. Photocatalytic efficiency remains unchanged during the first four cycles (Fig. 13). These results represent TCA(1.2) as a recyclable and promising photocatalyst for practical application.

4. Conclusion

In summary, a multicomponent photocatalytic system containing TiO_2 , Cu_2O , and different amounts of silver by a facile impregnation-calcination route combined with a photodeposition strategy was prepared. The obtained photocatalysts were characterized by different techniques such as XRD, DRS, N_2 physisorption, TEM, and FESEM/EDX. The prepared samples exhibited visible light photocatalytic activity for 2,4-DCP degradation as a consequence of Cu_2O and Ag synergetic effect. The introduction of Cu_2O and silver resulted in the improved visible-light absorption ability. Moreover, the SPR-induced local electric field would provide dual Z-scheme charge transfer in the composite, which enables both high separation efficiency and high redox potential of the generated electrons and holes. The present study demonstrated that the SPR effect of Ag can adjust the flow of the photogenerated electron-hole pairs and provide a deeper insight into the design of highly efficient photocatalysts for organic pollutant degradation. The degradation reactions follow first-order kinetics. Reuse of the best photocatalyst (TCA(1.2)) did not show any reduction in catalyst activity for 2,4-DCP degradation under visible light after four reaction cycles.

Acknowledgments

The authors wish to acknowledge the financial support of University of Tehran for supporting this research. Also, the authors wish to acknowledge the financial support of Iran Nanotechnology Initiative Council (INIC) Foundation (Grant no. 120865).

References

- [1] L. Liu, L. Ding, Y. Liu, W. An, Sh. Lin, Y. Liang, W. Cui, A stable $\text{Ag}_3\text{PO}_4/\text{PANI}$ core@shell hybrid: enrichment photocatalytic degradation with π - π conjugation, *Appl. Catal., B*, 201 (2017) 92–104.
- [2] L. Liu, Y. Qi, J. Lu, Sh. Lin, W. An, Y. Liang, W. Cui, A stable $\text{Ag}_3\text{PO}_4/\text{g-C}_3\text{N}_4$ hybrid core@shell composite with enhanced visible light photocatalytic degradation, *Appl. Catal., B*, 183 (2016) 133–141.
- [3] X. Wang, Y. Liang, W. An, J. Hu, Y. Zhu, W. Cui, Removal of chromium (VI) by a self-regenerating and metal free $\text{g-C}_3\text{N}_4/\text{graphene}$ hydrogel system via the synergy of adsorption and photo-catalysis under visible light, *Appl. Catal., B*, 219 (2017) 53–62.
- [4] F. Chen, W. An, L. Liu, Y. Liang, W. Cui, Highly efficient removal of bisphenol A by a three-dimensional graphene hydrogel- AgBr/rGO exhibiting adsorption/photocatalysis synergy, *Appl. Catal., B*, 217 (2017) 65–80.
- [5] Y. Liang, Sh. Lin, L. Liu, J. Hu, W. Cui, Oil-in-water self-assembled Ag/AgCl QDs sensitized Bi_2WO_6 : enhanced photocatalytic degradation under visible light irradiation, *Appl. Catal., B*, 164 (2015) 192–203.
- [6] W. Cui, W. An, L. Liu, J. Hu, Y. Liang, Novel Cu_2O quantum dots coupled flower-like BiOBr for enhanced photocatalytic degradation of organic contaminant, *J. Hazard. Mater.*, 280 (2014) 417–427.
- [7] A.J. Nozik, R. Memming, Physical chemistry of semiconductor-liquid interfaces, *J. Phys. Chem.*, 100 (1996) 13061–13078.
- [8] H.Y. Zhu, Y. Lan, X.P. Gao, S.P. Ringer, Z.F. Zheng, D.Y. Song, J.C. Zhao, Phase transition between nanostructures of titanate and titanium dioxides via simple wet-chemical reactions, *J. Am. Chem. Soc.*, 127 (2005) 6730–6736.
- [9] C. Burda, Y. Lou, X. Chen, A.C.S. Samia, J. Stout, J.L. Gole, Enhanced nitrogen doping in TiO_2 nanoparticles, *Nano Lett.*, 3 (2008) 1049–1051.
- [10] R. Yuan, T. Chen, E. Fei, J. Lin, Z. Ding, J. Long, Z. Zhang, X. Fu, P. Liu, L. Wu, Surface chlorination of TiO_2 -based photocatalysts: a way to remarkably improve photocatalytic activity in both UV and visible region, *ACS Catal.*, 1 (2011) 200–206.
- [11] H. Li, Z. Bian, J. Zhu, Y. Huo, H. Li, Y. Lu, Mesoporous Au/TiO_2 nanocomposites with enhanced photocatalytic activity, *J. Am. Chem. Soc.*, 129 (2007) 4538–4539.
- [12] L.Y. Hu, Y.M. Zhang, S.M. Zhang, B.X. Li, Synthesis, characterization and photocatalytic performance of mesoporous Si-N co-doped nano-spherical anatase TiO_2 with high thermal stability, *RSC Adv.*, 6 (2016) 43098–43103.
- [13] Y. Wang, J. Tao, X. Wang, Zh. Wang, M. Zhang, G. He, Zh. Sun, A unique $\text{Cu}_2\text{O}/\text{TiO}_2$ nanocomposite with enhanced

- photocatalytic performance under visible light irradiation, *Ceram. Int.*, 43 (2017) 4866–4872.
- [14] Y. Zhang, J. Zhu, X. Yu, J. Wei, L. Hu, S. Dai, The optical and electrochemical properties of CdS/CdSe co-sensitized TiO₂ solar cells prepared by successive ionic layer adsorption and reaction processes, *Sol. Energy*, 86 (2012) 964–971.
- [15] H.J. Lee, J. Bang, J. Park, S. Kim, S.-M. Park, Multilayered semiconductor (CdS/CdSe/ZnS)-sensitized TiO₂ mesoporous solar cells: all prepared by successive ionic layer adsorption and reaction processes, *Chem. Mater.*, 22 (2010) 5636–5643.
- [16] J. Shi, On the synergetic catalytic effect in heterogeneous nanocomposite catalysts, *Chem. Rev.*, 113 (2012) 2139–2181.
- [17] I. Robel, V. Subramanian, M. Kuno, P.V. Kamat, J. Am, Quantum dot solar cells. Harvesting light energy with CdSe nanocrystals molecularly linked to mesoscopic TiO₂ films, *Chem. Soc.*, 128 (2006) 2385–2393.
- [18] R. Dagherir, P. Drogui, D. Robert, Modified TiO₂ for environmental photocatalytic applications: a review, *Ind. Eng. Chem. Res.*, 52 (2013) 3581–3599.
- [19] Y. Wang, Q. Wang, X. Zhan, F. Wang, M. Safdar, J. He, Visible light driven type II heterostructures and their enhanced photocatalysis properties: a review, *Nanoscale*, 5 (2013) 8326–8339.
- [20] M. Hosseini, S. Siffert, H. Tidahy, R. Cousin, J.-F. Lamonier, A. Aboukais, A. Vantomme, M. Roussel, B.-L. Su, Stability and deactivation of Fe-ZSM-5 zeolite catalyst for catalytic wet peroxide oxidation of phenol in a membrane reactor, *Catal. Today*, 122 (2007) 391–396.
- [21] B. Kumar, S. Saha, A. Ganguly, A.K. Ganguli, A facile low temperature (350°C) synthesis of Cu₂O nanoparticles and their electrocatalytic and photocatalytic properties, *RSC Adv.*, 4 (2014) 12043–12049.
- [22] Z. Zheng, B. Huang, Z. Wang, M. Guo, X. Qin, X. Zhang, P. Wang, Y. Dai, Crystal faces of Cu₂O and their stabilities in photocatalytic reactions, *J. Phys. Chem. C*, 113 (2009) 14448–14453.
- [23] W.-C. Huang, L.-M. Lyu, Y.-C. Yang, M.H. Huang, Synthesis of Cu₂O nanocrystals from cubic to rhombic dodecahedral structures and their comparative photocatalytic activity, *J. Am. Chem. Soc.*, 134 (2011) 1261–1267.
- [24] C. Dong, M. Zhong, T. Huang, M. Ma, D. Wortmann, M. Brajdic, I. Kelbassa, Photodegradation of methyl orange under visible light by micro-nano hierarchical Cu₂O structure fabricated by hybrid laser processing and chemical dealloying, *ACS Appl. Mater. Interfaces*, 3 (2011) 4332–4338.
- [25] Q. Wang, K. Zhu, N.R. Neale, A.J. Frank, Constructing ordered sensitized heterojunctions: bottom-up electrochemical synthesis of p-type semiconductors in oriented n-TiO₂ nanotube arrays, *Nano Lett.*, 9 (2009) 806–813.
- [26] Y. Hou, X. Li, X. Zou, X. Quan, G. Chen, Photoelectrocatalytic activity of a Cu₂O-loaded self-organized highly oriented TiO₂ nanotube array electrode for 4-chlorophenol degradation, *Environ. Sci. Technol.*, 43 (2009) 858–863.
- [27] Z. Min, X. Wang, Y. Li, J. Jiang, J. Li, D. Qian, J. Li, A highly efficient visible-light-responding Cu₂O-TiO₂/g-C₃N₄ photocatalyst for instantaneous discolorations of organic dyes, *Mater. Lett.*, 193 (2017) 18–21.
- [28] H. Yuan, J. Liu, J. Li, Y. Li, X. Wang, Y. Zhang, J. Jiang, Sh. Chen, Ch. Zhao, D. Qian, Designed synthesis of a novel BiVO₄-Cu₂O-TiO₂ as an efficient visible-light-responding photocatalyst, *J. Colloid Interface Sci.*, 444 (2015) 58–66.
- [29] J. Xing, Z. Chen, F. Xiao, X. Ma, C. Wen, Z. Li, H. Yang, Cu-Cu₂O-TiO₂ nanojunction systems with an unusual electron-hole transportation pathway and enhanced photocatalytic properties, *Chem. Asian J.*, 8 (2013) 1265–1270.
- [30] X. Li, J. Yu, J. Low, Y. Fang, J. Xiaoc, X. Chen, Engineering heterogeneous semiconductors for solar water splitting, *J. Mater. Chem. A*, 6 (2015) 2485–2534.
- [31] H. Tada, T. Mitsui, T. Kiyonaga, T. Akita, K. Tanaka, All-solid-state Z-scheme in CdS-Au-TiO₂ three-component nanojunction system, *Nat. Mater.*, 5 (2006) 782–786.
- [32] H. Zhu, B. Yang, J. Xu, Z. Fu, M. Wen, T. Guo, S. Fu, J. Zuo, S. Zhang, Construction of Z-scheme type CdS-Au-TiO₂ hollow nanorod arrays with enhanced photocatalytic activity, *Appl. Catal., B*, 90 (2009) 463–469.
- [33] L. Zhang, K.H. Wong, Z. Chen, J.C. Yu, J. Zhao, C. Hu, C.Y. Chang, P.K. Wong, AgBr-Ag-Bi₂WO₆ nanojunction system: a novel and efficient photocatalyst with double visible-light active components, *Appl. Catal., A*, 363 (2009) 221–229.
- [34] X. Wang, S. Li, Y. Ma, H. Yu, J. Yu, H₂WO₄-H₂O/Ag/AgCl composite nanoplates: a plasmonic Z-scheme visible-light photocatalyst, *J. Phys. Chem. C*, 115 (2011) 14648–14655.
- [35] L. Ye, J. Liu, C. Gong, L. Tian, T. Peng, L. Zan, Two different roles of metallic Ag on Ag/AgX/BiOX (X = Cl, Br) visible light photocatalysts: surface plasmon resonance and Z-scheme bridge, *ACS Catal.*, 2 (2012) 1677–1683.
- [36] D. Xu, B. Cheng, S. Cao, J. Yu, Enhanced photocatalytic activity and stability of Z-scheme Ag₂CrO₄-GO composite photocatalysts for organic pollutant degradation, *Appl. Catal. B*, 164 (2015) 380–388.
- [37] X. Wang, G. Liu, Z. Chen, F. Li, L. Wang, G. Lu, Enhanced photocatalytic hydrogen evolution by prolonging the lifetime of carriers in ZnO/CdS heterostructures, *Chem. Commun.*, 23 (2009) 3452–3454.
- [38] P. Zhou, J.G. Yu, M. Jaroniec, All-solid-state Z-scheme photocatalytic systems, *Adv. Mater.*, 26 (2014) 4920–4935.
- [39] H. Tada, T. Mitsui, T. Kiyonaga, T. Akita, K. Tanaka, All-solid-state Z-scheme in CdS-Au-TiO₂ three-component nanojunction system, *Nat. Mater.*, 5 (2006) 782–786.
- [40] K. Xie, Q. Wu, Y. Wang, W. Guo, M. Wang, L. Sun, Electrochemical construction of Z-scheme type CdS/Ag/TiO₂ nanotube arrays with enhanced photocatalytic activity, *Electrochem. Commun.*, 13 (2011) 1469–1472.
- [41] X. Wang, G. Liu, L. Wang, Z. Chen, G. Lu, H. Cheng, ZnO/CdS@Cd heterostructure for effective photocatalytic hydrogen generation, *Adv. Energy Mater.*, 2 (2012) 42–46.
- [42] H. Lin, J. Cao, B. Luo, B. Xu, S. Chen, Synthesis of novel Z-scheme AgI/Ag/AgBr composite with enhanced visible light photocatalytic activity, *Catal. Commun.*, 21 (2012) 91–95.
- [43] H. Tada, T. Mitsui, T. Kiyonaga, T. Akita, K. Tanaka, All-solid-state Z-scheme in CdS-Au-TiO₂ three-component nanojunction system, *Nat. Mater.*, 5 (2006) 782–786.
- [44] H. Zhu, B. Yang, J. Xu, Z. Fu, M. Wen, T. Guo, S. Fu, J. Zuo, S. Zhang, Construction of Z-scheme type CdS-Au-TiO₂ hollow nanorod arrays with enhanced photocatalytic activity, *Appl. Catal., B*, 90 (2009) 463–463.
- [45] J. Fu, Sh. Cao, J. Yu, Dual Z-scheme charge transfer in TiO₂/Ag/Cu₂O composite for enhanced photocatalytic hydrogen generation, *J. Materiomics*, 1 (2015) 124–133.
- [46] U.G. Ahlborg, T.M. Thunberg, Chlorinated phenols: occurrence, toxicity, metabolism, and environmental impact, *Crit. Rev. Toxicol.*, 7 (1980) 1–35.
- [47] H.C. Lee, J.H. In, J.H. Kim, K.Y. Hwang, C.H. Lee, Kinetic analysis for decomposition of 2,4-dichlorophenol by supercritical water oxidation, *Korean J. Chem. Eng.*, 22 (2005) 882–888.
- [48] D.D. Dionysiou, A.P. Khodadoust, A.M. Kern, M.T. Suidan, I. Baudin, J.M. Laine, Continuous-mode photocatalytic degradation of chlorinated phenols and pesticides in water using a bench-scale TiO₂ rotating disk reactor, *Appl. Catal., B*, 24 (2000) 139–155.
- [49] K. Arnoldsson, P.L. Andersson, P. Haglund, Formation of environmentally relevant brominated dioxins from 2,4,6-tribromophenol via bromoperoxidase-catalyzed dimerization, *Environ. Sci. Technol.*, 46 (2012) 7239–7244.
- [50] J. Bandara, J.A. Mielczarski, A. Lopez, J. Kiwi, Sensitized degradation of chlorophenols on iron oxides induced by visible light comparison with titanium oxide, *Appl. Catal., B*, 34 (2001) 321–333.
- [51] X.D. Jiang, Y.P. Zhang, J. Jiang, Y. Rong, Y. Wang, Y. Wu, C. Pan, Characterization of oxygen vacancy associates within hydrogenated TiO₂: a positron annihilation study, *J. Phys. Chem.*, 116 (2012) 22619–22624.
- [52] M. Khan, W. Cao, Cationic (V, Y)-codoped TiO₂ with enhanced visible light induced photocatalytic activity a combined experimental, theoretical study, *J. Appl. Phys.*, 114 (2013) 183514.

- [53] W.X. Wei, W.D. Jian, L.X. Jun, Silver-doping induced lattice distortion in TiO₂ nanoparticles, *Chin. Phys. Lett.*, 7 (2009) 77809–77814.
- [54] M. Hamadani, A. Reisi-Vanani, A. Majedi, Sol-gel preparation and characterization of Co/TiO₂ nanoparticles application to the degradation of methyl orange, *J. Iran. Chem. Soc.*, 7 (2010) 52–58.
- [55] Y. Koo, G. Littlejohn, B. Collins, Y. Yun, V.N. Shanov, M. Schulz, D. Pai, J. Sankar, Synthesis and characterization of Ag–TiO₂-CNT nanoparticle composites with high photocatalytic activity under artificial light, *Composites Part B*, 57 (2014) 105–111.
- [56] M.S.A. Shah, K. Zhang, A.R. Park, K.S. Kim, N.-G. Park, J.H. Park, P.J. Yoo, Single-step solvothermal synthesis of mesoporous Ag–TiO₂-reduced graphene oxide ternary composites with enhanced photocatalytic activity, *Nanoscale*, 5 (2013) 5093–5101.
- [57] X. Zhou, G. Liu, J. Yu, W. Fan, Surface plasmon resonance-mediated photocatalysis by noble metal-based composites under visible light, *J. Mater. Chem.*, 22 (2012) 21337–21354.
- [58] S. Kumar, S. Khanchandani, M. Thirumal, A.K. Ganguli, Achieving enhanced visible-light-driven photocatalysis using type-II NaNbO₃/CdS core/shell heterostructures, *ACS Appl. Mater. Interfaces*, 6 (2014) 13221–13233.
- [59] S. Kaviya, J. Santhanalakshmi, B. Viswanathan, J. Muthumar, K. Srinivasan, Biosynthesis of silver nanoparticles using *Citrus sinensis* peel extract and its antibacterial activity, *Spectrochim. Acta, Part A*, 79 (2011) 594–598.
- [60] K.S.W. Sing, D.H. Everett, R.A.W. Haul, L. Moscou, R.A. Pierotti, Reporting physisorption data for gas/solid systems with special reference to the determination of surface area and porosity, *Pure Appl. Chem.*, 57 (1985) 603–619.
- [61] J. Li, S.K. Cushing, J. Bright, F. Meng, T.R. Senty, P. Zheng, A.D. Bristow, N. Wu, Ag@Cu₂O core-shell nanoparticles as visible-light plasmonic photocatalysts, *ACS Catal.*, 3 (2013) 47–51.
- [62] S. Chen, Y. Hu, L. Ji, X. Jiang, X. Fu, Preparation and characterization of direct Z-scheme photocatalyst Bi₂O₃/NaNbO₃ and its reaction mechanism, *Appl. Surf. Sci.*, 293 (2014) 357–366.
- [63] J.G. Yu, G.P. Dai, B.B. Huang, Fabrication and characterization of visible-light-driven plasmonic photocatalyst Ag/AgCl/TiO₂ nanotube arrays, *J. Phys. Chem. C*, 113 (2009) 16394–16401.
- [64] G. Begum, J. Manna, R.K. Rana, Controlled orientation in a bio-inspired assembly of Ag/AgCl/ZnO nanostructures enables enhancement in visible-light-induced photocatalytic performance, *Chem. Eur. J.*, 18 (2012) 6847–6853.
- [65] X. Jia, Y. Liu, J. Sun, H. Sun, Z. Su, X. Pan, R. Wang, Theoretical investigation of the reactions of CF₃CHFOCF₃ with the OH radical and Cl atom, *Phys. Chem. A*, 114 (2009) 417–424.
- [66] P. Wang, B.B. Huang, X.Y. Qin, X.Y. Zhang, Y. Dai, J.Y. Wei, M.H. Whangbo, Ag@AgCl: a highly efficient and stable photocatalyst active under visible light, *Angew. Chem., Int. Ed.*, 47 (2008) 7931–7933.
- [67] H. Xu, H.M. Li, J. Xia, S. Yin, Z. Luo, L. Liu, L. Xu, One-pot synthesis of visible-light-driven plasmonic photocatalyst Ag/AgCl in ionic liquid, *ACS Appl. Mater. Interfaces*, 3 (2011) 22–29.